JACS
JOURNAL OF THE AMERICAN CHEMICAL SOCIETY
Article
pubs.acs.org/JACS

Fluorine Substituents Reduce Charge Recombination and Drive Structure and Morphology Development in Polymer Solar Cells

Andrew C. Stuart,[†] John R. Tumbleston,[‡] Huaxing Zhou,[†] Wentao Li,[†] Shubin Liu,[§] Harald Ade,[‡] and Wei You*[,†]

[†]Department of Chemistry, University of North Carolina at Chapel Hill, Chapel Hill, North Carolina 27599-3290, United States
[‡]Department of Physics, North Carolina State University, Raleigh, North Carolina 27695, United States
[§]Research Computing Center, University of North Carolina at Chapel Hill, Chapel Hill, North Carolina 27599-3420, United States

Supporting Information

ABSTRACT: Three structurally identical polymers, except for the number of fluorine substitutions (0, 1, or 2) on the repeat unit (BnDT-DTBT), are investigated in detail, to further understand the impact of these fluorine atoms on open circuit voltage (V_{oc}), short circuit current (J_{sc}), and fill factor (*FF*) of related solar cells. While the enhanced V_{oc} can be ascribed to a lower HOMO level of the polymer by adding more fluorine substituents, the improvement in J_{sc} and *FF* are likely due to suppressed charge recombination. While the reduced bimolecular recombination with raising fluorine concentration is confirmed by variable light intensity studies, a plausibly suppressed geminate recombination is implied by the significantly increased change of dipole moment between the ground and excited states ($\Delta\mu_{ge}$) for these polymers as the number of fluorine substituents increases. Moreover, the 2F polymer (PBnDT-DTffBT) exhibits significantly more scattering in the in-plane lamellar stacking and out-of-plane $\pi-\pi$ stacking directions, observed with GIWAXS. This indicates that the addition of fluorine leads to a more face-on polymer crystallite orientation with respect to the substrate, which could contribute to the suppressed charge recombination. R-SoXS also reveals that PBnDT-DTffBT has larger and purer polymer/fullerene domains. The higher domain purity is correlated with an observed decrease in PCBM miscibility in polymer, which drops from 21% (PBnDT-DTBT) to 12% (PBnDT-DTffBT). The disclosed "fluorine" impact not only explains the efficiency increase from 4% of PBnDT-DTBT (0F) to 7% with PBnDT-DTffBT (2F) but also suggests fluorine substitution should be generally considered in the future design of new polymers.

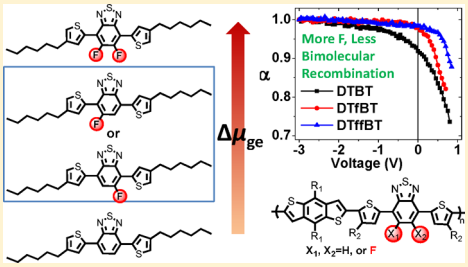

INTRODUCTION

Fluorine atoms substituted directly to the backbone of conjugated polymers have shown great promise in enhancing the efficiency of polymer-based bulk heterojunction (BHJ) solar cells.[1−13] For example, fluorine substituents have been identified as the *single* performance-enhancing factor in three of the highest performing polymers.[1−3] A detailed comparison of these three polymers and their nonfluorinated analogues has been highlighted by a recent review article.[13] However, the cause for the efficiency improvement varies noticeably, depending upon specific systems. It is generally true that the electron-withdrawing nature of these fluorine substituents, when directly on the conjugated backbone, lowers the HOMO energy level of conjugated polymers. This can translate into an enhanced open circuit voltage (V_{oc}) in BHJ solar cells, which essentially accounts for the efficiency increase in certain systems.[1,6,8] However, in other reported systems,[2,3,7,9,10] it appears that fluorinated polymer also demonstrates a noticeably improved short circuit current (J_{sc}) and/or fill factor (*FF*) in BHJ devices versus those of the nonfluorinated analogue polymer-based devices—a very interesting behavior that warrants further investigation. More importantly, the improvement of J_{sc} and/or *FF* has been the *dominating* factor in the efficiency enhancement in these systems,[2,3,7,9,10] as opposed to the V_{oc} enhancement as the major boost for efficiency in other systems.[1,6,8] Therefore the intriguing "fluorine" impact has been under intensive research, aiming to uncover the underlying working principles.[11,14−17]

As our attempt to further understand the "fluorine" impact, we selected one such system, poly[benzo[1,2-*b*:4,5-*b*′]-dithiophene-*alt*-5,6-difluoro-4,7-dithien-2-yl-2,1,3-benzothiadiazole] (PBnDT-DTffBT) ("2F") and its nonfluorinated analogue, PBnDT-DTBT ("0F"), for an in-depth study. In our original report,[2] we found the fluorinated polymer ("2F") not only exhibited an increased V_{oc}, but also enhanced J_{sc} and *FF* in its BHJ devices. To complete this series, we further synthesized a new polymer with a singly substituted fluorine on the repeat unit, PBnDT-DTfBT ("1F"), and carefully investigated all three polymers in a comparative manner (see Figure 1). In this contribution, we show how increasing the concentration of fluorine atoms boosts the performance of conventional photovoltaic characteristics (V_{oc}, J_{sc}, and *FF*) in this series of polymers. Further, we reveal that these fluorine

Received: September 19, 2012
Published: January 4, 2013

   dx.doi.org/10.1021/ja309289u | J. Am. Chem. Soc. 2013, 135, 1806−1815

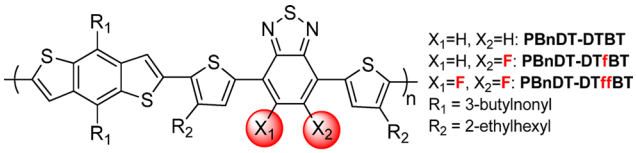

Figure 1. The structures of PBnDT-DTBT ("0F"), -DTfBT ("1F") and -DTffBT ("2F").

atoms reduce bimolecular recombination, i.e., the recombination of two free carriers (a hole and electron) that were generated by different absorption events, through improved polymer organization, increased purity of polymer-rich and fullerene-rich domains, and a reduction in molecular miscibility. In addition, increasing the number of fluorine substitutions from 0 to 2 leads to a noticeable increase in the change of dipole moment from the ground state to the excited state ($\Delta\mu_{ge}$), which likely helps suppress geminate recombination, i.e., the recombination of an electron−hole pair that failed to dissociate, and improve charge separation. Therefore, the suppression of recombination losses and formation of advantageous morphological and structural changes both constitute the "fluorine" impact.

RESULTS AND DISCUSSION

Synthesis and Optical and Electrochemical Properties of Polymers. Both DTBT and DTffBT monomers were synthesized as previously reported,[2] and the synthesis of DTfBT monomer is described in the Supporting Information (Scheme S1). Previous studies have shown that the positioning and size of solubilizing side chains can have a large effect on the number average molecular weight (M_n) and photovoltaic properties of devices.[18−22] With this polymer series, we used identical side-chain positioning and structures to minimize these effects, thereby allowing us to focus solely on the impact introduced by the fluorine substitutions. Additionally, we optimized the polymerization and purification of each polymer to yield a similar M_n and polydispersity index (PDI), as shown in Table 1. Details of polymerization and purification procedures are provided in the Supporting Information (SI).

Table 1. Key Properties of Polymers (Molecular Weight, Optical Properties, and HOMO Level) and V_{oc} of Related BHJ Devices

polymer	M_n/PDI[a] [kg/mol]	film E_g[b] [eV]	abs. coef.[c] [cm^{-1}]	HOMO[d] [eV]	meas. V_{oc} [V]
DTBT	52.4/2.0	1.65	4.0×10^4	−5.42	0.81
DTfBT	39.3/1.9	1.67	4.0×10^4	−5.48	0.85
DTffBT	39.1/2.1	1.73	4.4×10^4	−5.53	0.91

[a]Determined by GPC in 1,2,4-trichlorobenzene at 150 °C. [b]Band gap calculated from the onset of the absorption of the solid film. [c]Measured from film absorption spectra at λ_{max} [d]Measured by cyclic voltammetry

Thickness-corrected absorption spectra of neat films of the 0F, 1F, and 2F polymers are displayed in Figure 2. The absorption spectra of all three polymers are quite similar, yielding only slightly different optical band gaps of 1.65, 1.67, and 1.73 eV for the 0F, 1F, and 2F polymers, respectively. Interestingly, there is a slight increase in bandgap as more fluorines are added. Notably, the doubly fluorinated 2F polymer yields an absorption coefficient of 4.4×10^{-4} cm^{-1}, slightly

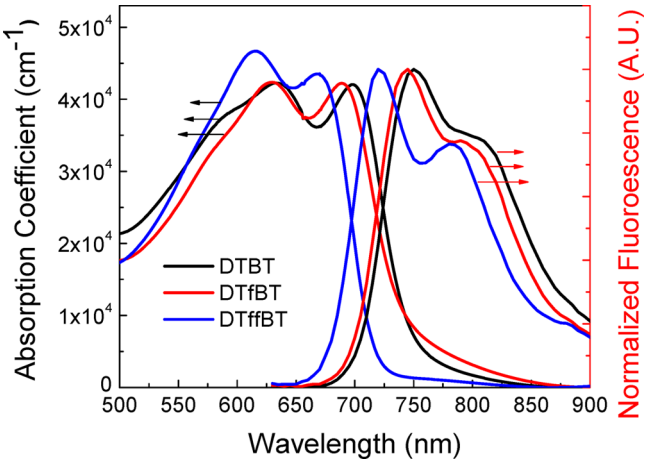

Figure 2. UV−vis absorption and fluorescence emission spectra of 0F (PBnDT-DTBT), 1F (PBnDT-DTfBT), and 2F (PBnDT-DTffBT) polymers in thin films.

higher than those for both 0F and 1F polymers (~4.0×10^{-4} cm^{-1}). This slight increase in absorption for 2F can be attributed to it having larger crystallites with a more face-on orientation, as discussed in the device morphology section.[23] Fluorescence characteristics of these three polymers were probed by subjecting the film of each polymer to an excitation at 600 nm, and these fluorescence spectra are displayed along with the absorption spectra in Figure 2 for facile approximation of the Stokes shift. All three polymers show similar Stokes shifts of 0.11−0.12 eV, which indicates that reorganizational free energy does not play a role in any observed difference of charge carrier dynamics among the three polymers.

To discern any differences in electrochemical ionization potentials, neat films of each polymer were deposited onto a glassy carbon electrode and scanned with a potentiostat. The HOMO energy levels of all polymers were approximated from the onset of the oxidation peak in each voltammogram (see SI Figure S5), and are listed in Table 1. The observed HOMO levels of the 0F polymer (−5.42 eV) and 2F polymer (−5.53 eV) match previously reported results, while the singly substituted 1F polymer yielded a HOMO level of −5.48 eV, in between those of 0F and 2F polymers. These results indicate that the HOMO energy level scales with increasing the number of fluorine substituents, correlating well with the observed increase in V_{oc} also shown in Table 1.

These results indicate that all three polymers possess very similar intrinsic polymer properties, except the slightly enhanced absorption coefficient of the doubly fluorinated polymer PBnDT-DTffBT and the increase on the HOMO level with the increase of the number of fluorine substituents.

Photovoltaic Properties. Photovoltaic devices were fabricated by spin-casting a blended solution of the polymer and PCBM ([6,6]-phenyl-C61-butyric acid methyl ester) onto a PEDOT:PSS-coated ITO electrode and then capping the device with 30 nm of calcium followed by 70 nm of aluminum. After determining the optimal polymer:PCBM ratio to be 1:1 for all three polymers, solar cell devices with three different active layer thicknesses (100, 150, and 200 ± 10 nm) were fabricated and tested, and results were compared. Since the film thickness of BHJ cells usually has a strong impact on the observed photovoltaic properties, our practice—comparing each polymer at similar film thickness rather than at whichever thickness yields optimal device efficiency—can ensure a more

dx.doi.org/10.1021/ja309289u | J. Am. Chem. Soc. 2013, 135, 1806−1815

fair evaluation. More importantly, these thickness-dependent data for all three polymers offer a rich data set to further probe the "fluorine" impact. For example, we have observed that in another fluorinated polymer,[3] the J_{sc} continues to increase as the active layer thickness is increased.

For each device, the $I-V$ curves were acquired under simulated 1 Sun condition (AM 1.5) and typical photovoltaic characteristics (V_{oc}, J_{sc}, and FF) are displayed in Table 2.

Table 2. PV Response of 1:1 Polymer:$PC_{61}BM$

polymer	thickness [nm ±10]	V_{oc} [V]	J_{sc} [mA/cm^2]	FF [%]	$\eta_{average}$ (η_{max}) [%]
DTBT	200	0.81	10.1	38.3	3.14 (3.50)
	150	0.79	11.0	44.2	3.84 (4.07)
	100	0.78	11.7	47.6	4.33 (4.53)
DTfBT	200	0.83	11.2	46.5	4.46 (4.77)
	150	0.85	11.4	50.6	4.91 (5.28)
	100	0.84	11.5	52.2	4.91 (5.22)
DTffBT	200	0.91	11.9	52.1	5.63 (6.05)
	150	0.91	12.7	56.2	6.51 (6.78)
	100	0.90	12.2	62.1	6.64 (7.16)

Analysis of the data in the table reveals both strong thickness dependence within each polymer series, and significant fluorine substitution dependence, manifested most notably in J_{sc} and FF. Below, we discuss in detail each of the three performance parameters that dictate device performance, V_{oc}, J_{sc}, and FF.

The origin of the V_{oc} has previously been related to the energy difference between the LUMO of the fullerene acceptor and the HOMO of the donor polymer[24,25] so long as there is good ohmic contact between the active layer and device electrodes.[26] This value, $(E_{LUMO(fullerene)} - E_{HOMO(polymer)})/e$, represents the maximum achievable voltage from a BHJ device but is rarely observed due to losses originating from band offsets, internal space charge, and molecular reorganizational energy characterized by the Stokes shift.[27] Both Table 2 and Figure 3a show that increasing the number of fluorine substituents enhances the observed V_{oc} of photovoltaic devices. Importantly, the V_{oc} increases nearly the same amount as the HOMO level is reduced with the fluorine substitution, indicating this is the sole cause of the enhanced V_{oc}. Furthermore, the Stokes shift is identical for all three polymers, and the measured V_{oc} is nearly identical for the same blend with different active layer thicknesses, indicating that molecular reorganizational energy and space charge differences, respectively, do not play a significant role in the V_{oc} differences.

On the other hand, J_{sc} displays interesting trends, depending upon the thickness and the number of fluorine substitutions as shown in Figure 3b. Typically, as the thickness of the active layer is increased over 100 nm, these polymer-based BHJ devices absorb more photons, which should generate additional charge carriers and thereby an enhanced J_{sc}. However, the usually concomitant increases in space charge and bimolecular recombination very often culminate in an overall net loss in J_{sc}. This net loss behavior can be observed in the 0F-based devices, with the J_{sc} dropping from 11.7 to 10.1 mA/cm^2 as device thickness is increased from 100 to 200 nm. However, when fluorine substituents are introduced onto the polymer backbone, losses in J_{sc} due to increased film thickness appear to be mitigated. For example, as film thickness is increased from 100 to 200 nm, the J_{sc} remains nearly constant for both 1F and 2F polymers. Therefore, at 200 nm, we observe an overall increase in J_{sc} as the number of fluorine substituents increases, from the

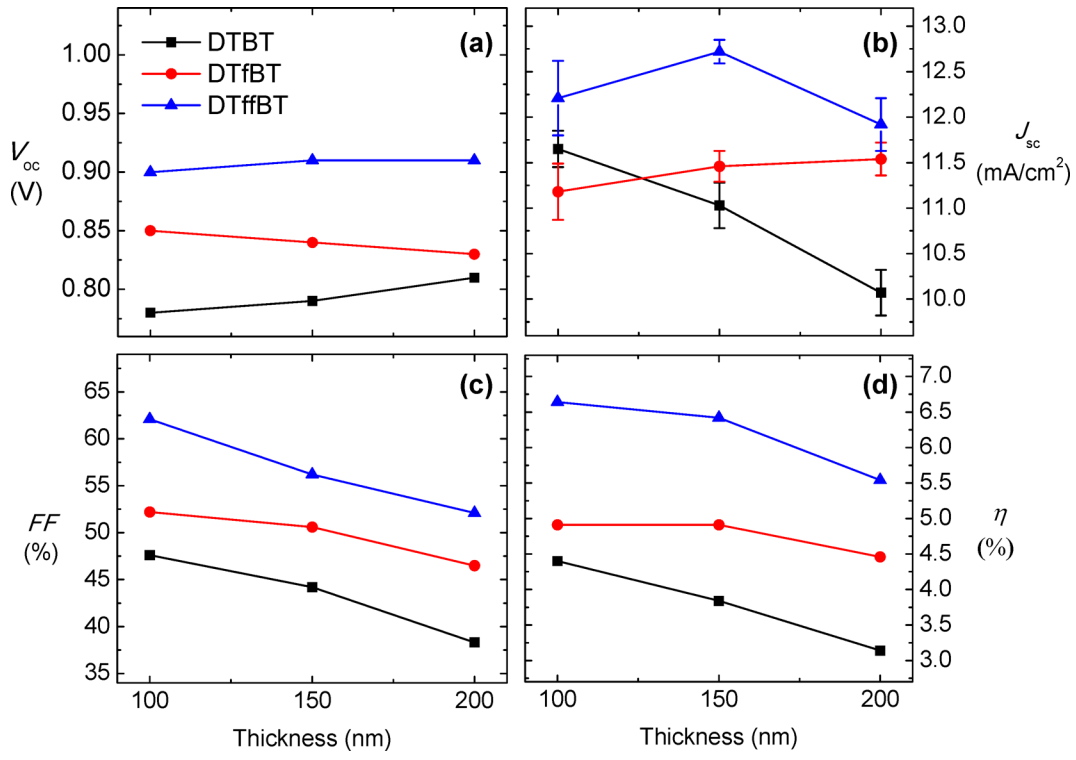

Figure 3. Fluorine concentration (0F, 1F, 2F) and thickness of the active layer (100, 150, 200 nm) are varied, and their effect on (a) V_{oc}, (b) J_{sc}, (c) FF, and (d) η are shown. Thickness measurements are ±10 nm.

dx.doi.org/10.1021/ja309289u | J. Am. Chem. Soc. 2013, 135, 1806−1815

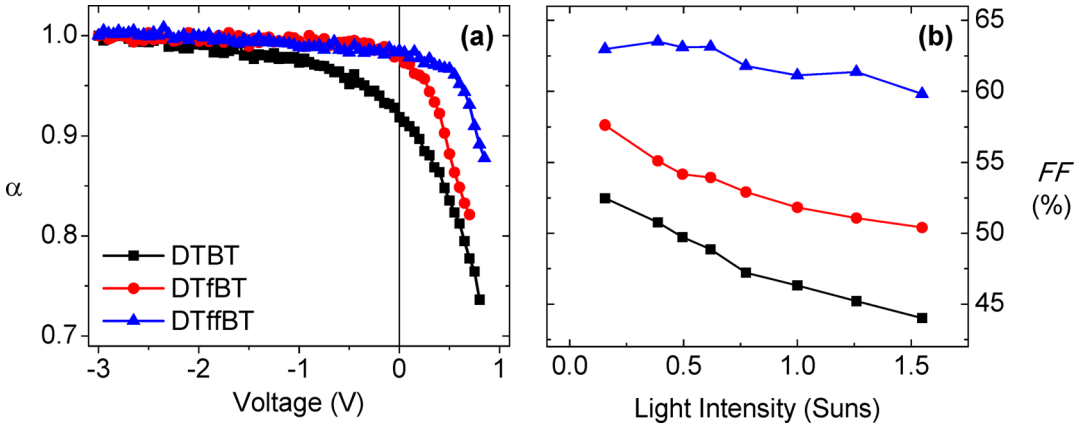

Figure 4. (a) Scaling exponent vs voltage for 0F-, 1F-, and 2F-based BHJ devices with 200 nm film thickness and (b) *FF* as function of light intensity for 100 nm thick films.

0F (10.1 mA/cm^2) to 2F-based devices (11.9 mA/cm^2). Similar trends have been observed in other fluorinated polymers,[3] where a noticeable increase of J_{sc} in the fluorinated polymer-based devices was partially ascribed to an increased hole mobility by the fluorine substitution. However, in the current series of polymers, the hole mobility is unlikely responsible for the increased J_{sc}, since the measured hole mobility by space charge limited current[28] (SCLC) (see SI Figure S6) does not vary significantly (average mobility for 0F, 1F, and 2F are 3.0, 2.9, and 3.6 × 10^{-4} cm^2/V·s, respectively). A more plausible explanation is the suppression of recombination losses with the introduction of these fluorine atoms (vide infra).

Typically, charge recombination losses manifest themselves most significantly in the *FF* of PV devices, as the *FF* is determined at voltages where the internal electric field is weak and carriers are not readily swept out of the active layer.[29] Looking at Figure 3c, *FF* is greatly affected not only by active layer thickness but also by the number of fluorine substitutions. Comparing the *FF* plot to the efficiency curves in Figure 3d, it is clear that of the three major photovoltaic parameters, *FF* appears to have the greatest influence on device power conversion efficiency. Most significantly, for the 100 nm thickness, the 2F-based devices exhibit the highest *FF* of 62%, as opposed to only 52% and 48% for the 0F- and 1F-based devices, respectively. This trend continues as the thickness of the active layer increases, with the 0F-based devices dropping to a mere 38% *FF* at 200 nm, while both fluorinated polymer-based devices still achieve respectable values. This implies that increasing fluorine substituents suppresses charge recombination losses in BHJ devices for this series of polymers.

Bimolecular Recombination. In order to further determine which loss mechanisms are causing the noted differences in *FF* and efficiency as the number of fluorine substituents are varied, we first measured photovoltaic performance under variable light intensity (P_{light}) between 0.2 and 1.5 suns. This technique is a simple probe for bimolecular recombination of free charges that can limit the photocurrent. If minimal bimolecular recombination occurs, the number of charge carriers collected and therefore the photocurrent should scale linearly with the light intensity.[30,31] On the other hand, a sublinear scaling of the photocurrent with light intensity would indicate a fraction of the charge carriers are lost during transport due to bimolecular recombination. Experimentally, by measuring the photocurrent (J_{photo}) at different values of P_{light}, bimolecular recombination can be quantified as a function of applied voltage by fitting a power law scaling exponent, α, via

$$J_{photo} = \beta(P_{light})^{\alpha} \quad (1)$$

where β is a constant. As the number of fluorine atoms is increased, the light intensity measurements in Figure 4a show a stark increase in α, which represents a decrease in bimolecular recombination, near maximum power point (~0.5 V). This reduction in bimolecular recombination with fluorine addition helps explain the enhanced *FF* as observed in Figure 3c and Figure 4b. While Figure 3c has been discussed earlier, Figure 4b shows not only a higher absolute *FF* for 2F polymer-based devices under all tested light intensities but also an insensitivity of *FF* to light intensity for 2F polymer-based devices. This means that, as the number of free carriers increases via a higher P_{light}, blends with a greater number of fluorine substituent atoms are able to stifle recombination and avoid *FF* losses. Overall, the light intensity dependence of J_{photo} and *FF* indicates that, at maximum power point, bimolecular recombination is indeed weakest in the devices with the 2F polymer and increases as the number of fluorine substitutes is reduced.

Differences in bimolecular recombination losses are not limited to maximum power point and also influence J_{sc}. As the applied voltage is decreased to strengthen the internal electric field and sweep out more of the charge carriers, α increases for all devices. There is low bimolecular recombination at short circuit conditions for the 1F- and 2F-based devices since $\alpha \approx 1$, while those based on the 0F polymer only achieve minimal recombination for higher electric fields near −3 V bias. At short circuit, α = 0.92 for the 0F-based solar cells, which indicates that J_{sc} is restricted due to this loss mechanism. Therefore, we identify bimolecular recombination as a photocurrent loss process that is sensitive to the number of fluorine substituents on the polymer backbone. Changes in this recombination process help explain the observed enhancement in *FF* when moving from 0F- to 1F- to 2F-based devices.

Structural Analysis and Modeling. Having established that fluorine substituents reduce recombination losses (especially bimolecular recombination) in these polymer-based BHJ solar cells, we next attempted to correlate this observation with the molecular structures of these polymers. It has been recently proposed by Yu et al. that the change of the dipole moment from the ground state to the excited state ($\Delta\mu_{ge}$) of the conjugated polymer largely correlates with the

dx.doi.org/10.1021/ja309289u | J. Am. Chem. Soc. 2013, 135, 1806−1815

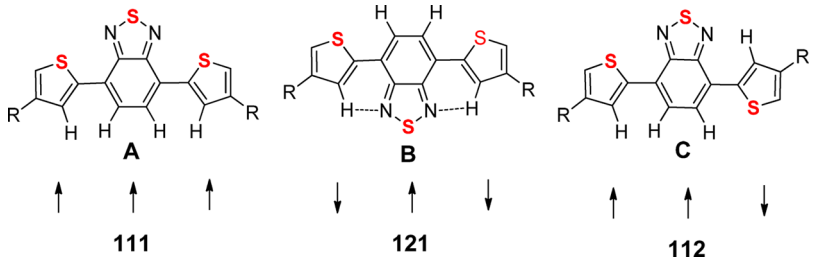

Figure 5. Possible conformations of the DTBT structural unit with annotation. "1" denotes the sulfur atom appearing on the top, "2" for the sulfur appearing on the bottom.

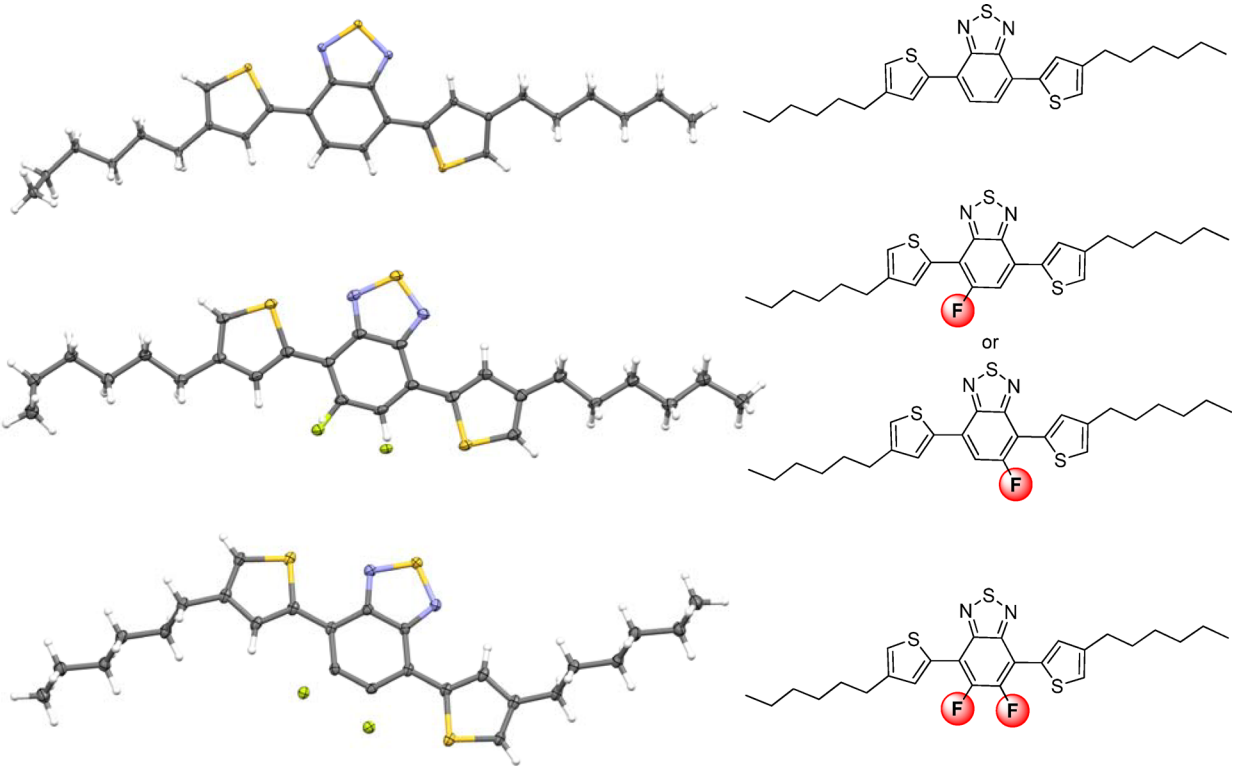

Figure 6. Crystal structures of model compounds of DTBT, DTfBT, and DTffBT. Hexyl chains were used instead of 2-ethylhexyl in order to grow single crystals. Due to its asymmetry by the single fluorine substituent, DTfBT has two possible conformers, both of which were identified in the crystal structure, with F7 and F8 appearing with 50% probability.

efficiency of related polymer-based solar cells.[15,32] They postulated that a larger $\Delta\mu_{ge}$ lowers the Coulombic binding energy of excitons and facilitates charge separation. Interestingly, it was also shown that the *FF* (and the efficiency) of BHJ devices shows a linear relationship with the ratio between the amplitude coefficients of pseudo-charge-transfer state (PCT) and charge-separated state (CS) of these polymer:PCBM blends[16] and that ratio was affected by the $\Delta\mu_{ge}$. All these prompted us to further investigate the impact on the dipole moment of PBnDT-DTBT polymers by fluorination.

To minimize the computing time and obtain more accurate results, we first needed to determine the conformation of the structural unit of our polymers, BnDT-DTBT, as the input for computational study. Because the flanking thiophenes of DTBT are alkylated, it is reasonable to assume a "trans" conformation between the alkylated thiophene (of DTBT) and the fused thiophene of BnDT in order to minimize the steric hindrance[33] (as indicated in Figure 7), similar to the "trans" conformation observed for other oligothiophenes.[34,35] So we turned our attention to resolving the conformation of the DTBT unit. The first conformer, **111** as shown in Figure 5, was implied by Yamashita et al. when they reported the crystal structure of a structurally related compound[36] but with selenadiazole in the center instead of benzothiadiazole. The second conformer, **121**, has been prevailing in the literature, presumably due to the fact that such a conformer could avoid steric hindrance coming from hydrogen atoms of thiophene and benzene and a plausible hydrogen bonding between the hydrogen of the thiophene and the central benzodithiazole. This plausible conformation was also implied by the crystal structure of another remotely structurally related compound.[37] A more definitive evidence to the conformer **121** came from a very recent work by Takimiya et al., where they reported the crystal structure of DTBT with methylated thiophenes as adopting the **121** conformation.[38] Additionally, there is a third possibility, **112** (or its identical isomer, **122**), combining features of **111** and **121**, which could exist as well.

In order to *definitively* determine the conformation of alkylated DTBT (especially upon fluorination), we synthesized three related molecules with 0, 1, or 2 fluorine substitutions

dx.doi.org/10.1021/ja309289u | J. Am. Chem. Soc. 2013, 135, 1806−1815

(Figure 6) and obtained related single crystals for X-ray diffraction analysis. Strikingly, all obtained crystal structures are structurally identical to the conformer **112**, i.e., the flanking two thienyls always in *opposite* direction, while maintaining a high planarity of the DTBT unit, regardless of the number of fluorine substituents (0, 1, or 2). This seemingly surprising result in fact gives a pseudolinear shape of the conjugated backbone (top image of Figure 7), which would help an

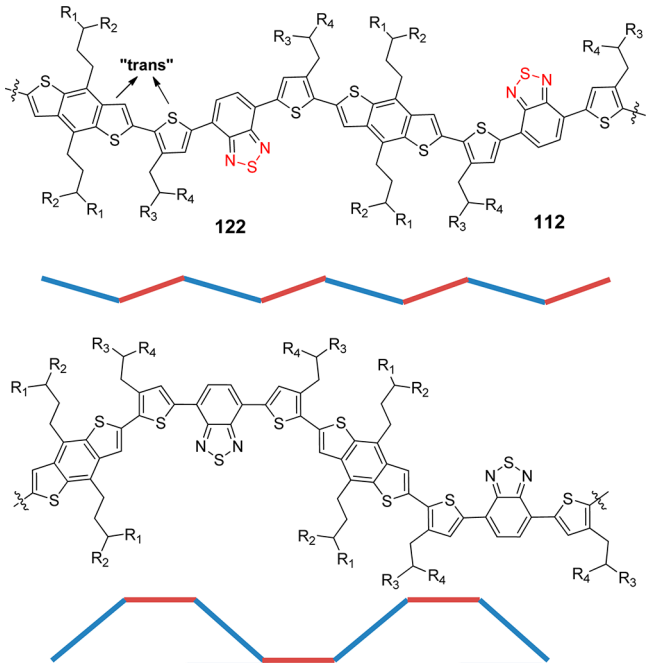

Figure 7. (Top) Proposed conformation of conjugated backbone (2 repeat units of BnDT-DTBT as shown), and the schematic showing the pseudo linear backbone. (Bottom) Other possible conformations, and a more curved conjugated backbone.

effective packing/stacking of these polymers and thereby improve the charge carrier mobility.[39] On the other hand, other possible conformers of DTBT (**111** or **121**) would lead to a more curved backbone with a possibility of reducing the mobility.[40,41] It should also be noted that this result, although in contrast to the crystal structure reported by Takimiya et al.,[38] may indicate that the inclusion of longer alkyl chains can actually improve chain packing and polymer organization.

Next, we subjected the more probable conformation of these conjugated backbones (top conformer in Figure 7) to quantum mechanical calculations at the theory level of B3LYP/6-311+G(d).[42,43] Time-dependent density functional theory with the same functional and basis set was employed to obtain the optimized excited state structure for the D−A repeat unit. The calculated dipole moments for both the ground (μ_g) and first excited (μ_e) states with one D−A repeat unit for each studied polymer are listed in Table 3. The noticeably large μ_e for all three polymers is because the LUMO is rather localized from our calculation. This suggests that there is a charge separation in the excited state, leading to the substantial increase of the dipole moment. The optimized structure and calculated frontier orbitals (HOMO and LUMO) for all three polymers are summarized in the SI (Figure S15). Interestingly, the μ_g of the BnDT-DTffBT (repeat unit of the 2F polymer) is noticeably smaller than that of its mono- or nonfluorinated counterpart. However, its dipole moment at the excited state is

Table 3. Calculated Dipole Moments of Monomers for All Three Polymers[a]

repeat unit	μ_g (debye)	μ_e (debye)	$\Delta\mu_{ge}$ (debye)
BnDT-DTBT	1.54	12.10	11.20
BnDT-DTfBT	1.49	14.10	15.18
BnDT-DTffBT	0.75	15.50	16.02

[a] μ_g and μ_e represent the dipole moment at ground state and excited state, respectively. $\Delta\mu_{ge}$ indicates the change in dipole moment between the ground state and the excited state, calculated by $\Delta\mu_{ge} = [(\mu_{gx} - \mu_{ex})^2 + (\mu_{gy} - \mu_{ey})^2 + (\mu_{gz} - \mu_{ez})^2]^{1/2}$, following reference 15.

the largest among all three studied polymers. Therefore, when focusing on the *change* of the dipole moment ($\Delta\mu_{ge}$), the fluorinated polymers (1F and 2F) have larger $\Delta\mu_{ge}$ than that of the nonfluorinated analogue (0F). The larger $\Delta\mu_{ge}$ of these fluorinated polymers could weaken the exciton binding energy and promote the formation of the charge-separated state, similar to what Yu et al. observed in their studies,[16] although further experiments on these polymers need to be carried out. Nevertheless, the (possibly) hindered geminate recombination by the larger $\Delta\mu_{ge}$, together with reduced bimolecular recombination (vide supra), can explain the much improved *FF* and J_{sc} as the number of F substitutions increases on the conjugated backbone, since both geminate and bimolecular recombination negatively impact these performance parameters.[11,44]

Device Morphology. On the basis of the noted changes in dipole moment at the molecular level, it is possible that the molecular energetics could drive the formation of different BHJ morphologies. Using various X-ray characterization techniques, we determined the crystalline structure and domain characteristics of blend films along with the miscibility of PCBM in each polymer. Thin films identical to those used for BHJ devices (~150 nm active layers allowed to dry in a closed Petri dish) were prepared on PEDOT:PSS-coated silicon wafers and characterized with grazing incidence wide-angle X-ray scattering (GIWAXS) at beamline 7.3.3 of the Advanced Light Source[45] to probe crystalline regions of the blend films. Two dimensional (2D) GIWAXS scattering data along with out-of-plane and in-plane 20° sector averages are shown in Figure 8. The (100) lamellar *d*-spacing corresponds to 18 Å and does not significantly change with fluorine substitution. Likewise, GIWAXS of the pure polymer films (see SI Figure S16) reveals that *d*-spacing does not change with addition of PCBM, which indicates that no PCBM intercalation occurs between the crystalline polymer chains as has been observed for other systems.[46] While addition of fluorine does not alter *d*-spacing, the relative orientation and crystal peak widths are modified when going from the 2F-based blends to those based on 0F or 1F. For instance, 2F-based blends show significant scattering in the in-plane (100) direction compared to the single and nonfluorinated blend films. Likewise, the (010) $\pi-\pi$ stacking peak at q = 1.6 Å^{-1} in the out-of-plane direction is only evident for blends of 2F polymer:PCBM. This indicates that double fluorination causes the polymer crystallites to adopt a higher proportion of face-on orientation with the side chains parallel to the substrate when compared with the other two blend films, a result consistent with previous work involving polymer fluorination.[17] Furthermore, the crystal peak widths decrease with addition of fluorine substituents, likely indicative of a reduction in paracrystallinity. Even so, the ordering in these materials is expected to be relatively poor compared with

dx.doi.org/10.1021/ja309289u | J. Am. Chem. Soc. 2013, 135, 1806−1815

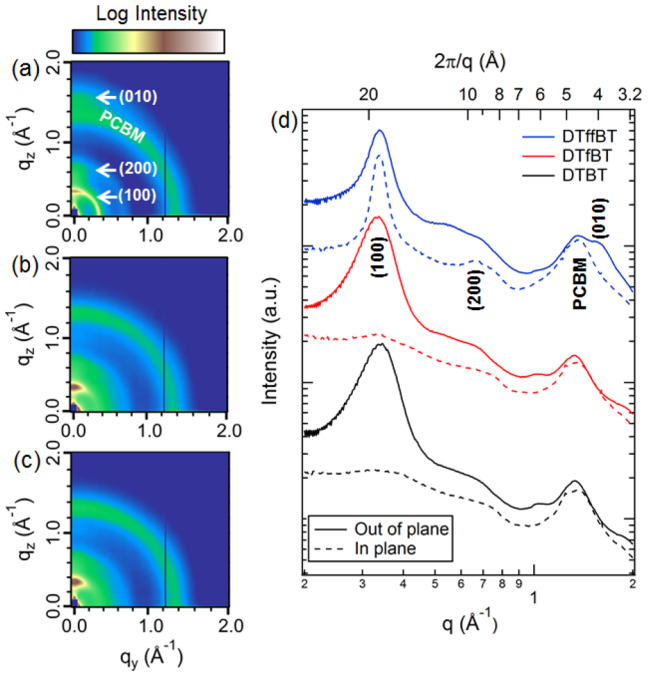

Figure 8. Two dimensional (2D) GIWAXS data for blend films based on (a) 2F, (b) 1F, and (c) 0F polymers. (d) In-plane and out-of-plane 20° sectors with the polymer peaks labeled along with the typical scattering contribution from PCBM. Please note that the 2D data have not been corrected for the "missing wedge" of data along the out-of-plane direction.

polymers such as poly(3-hexylthiophene), since multiple and sharp higher diffraction order peaks are not observed.[47] Overall, these results indicate that addition of two fluorine substituent atoms causes a change in the polymer paracrystallinity and crystallite orientation in the blend films. The relevance to device performance will be discussed below.

While GIWAXS measurements provide valuable insights into the structure of the polymer/fullerene blends, it is only sensitive to the crystalline regions. However, amorphous regions not probed with GIWAXS can play an important role in device function, especially since molecular miscibility has been demonstrated for many BHJ systems.[48,49] To gain a more complete picture of film morphology, the distributions of domain spacing along with relative domain purities were assessed with resonant soft X-ray scattering (R-SoXS)[50,51] at beamline 11.0.1.2 of the Advanced Light Source.[52] This technique utilizes the unique optical contrast between polymer and fullerene near the carbon 1s absorption edge ($h\nu \approx 280$ eV). Using the dispersive (δ) and absorptive (β) parts of the complex index of refraction, $\tilde{n} = 1 - \delta + i\beta$, for the polymers and PCBM (see SI Figure S20), the scattering contrast as a function of photon energy is shown in Figure 9b for the 2F polymer and PCBM. The contrast is determined by the differences in δ and β and is proportional to $(\Delta\delta)^2 + (\Delta\beta)^2$. Also displayed in Figure 9b is the contrast between polymer and fullerene with vacuum, which represents scattering due to mass−thickness variations, such as surface roughness or thickness variations.

Figure 9a shows the angle-integrated 2D scattering data for photon energies of 270.0 and 284.0 eV. The circular average intensity has been multiplied by q^2 to correspond to the azimuthal integration of the 2D data. The scattering profiles are different depending on the photon energy owing to the

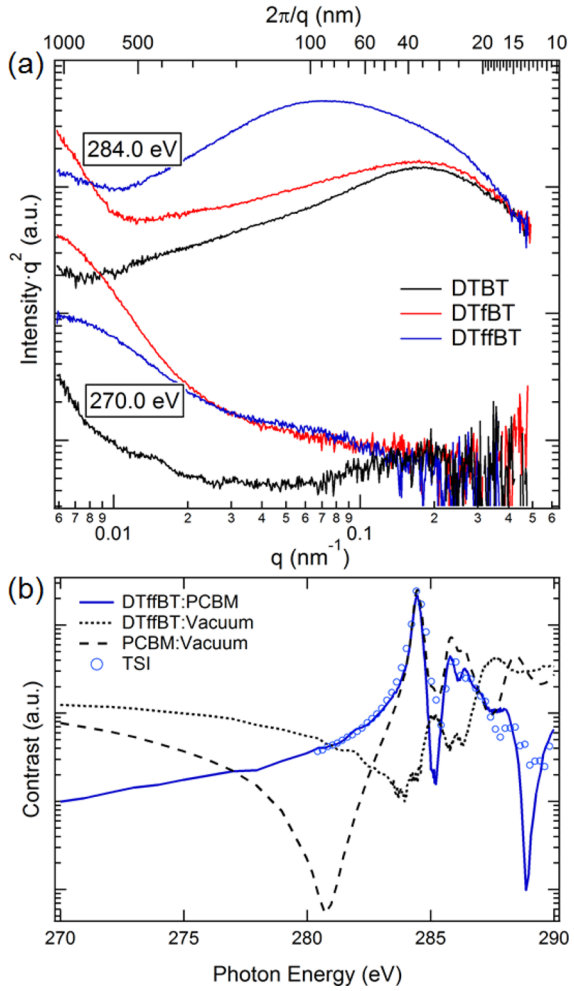

Figure 9. (a) R-SoXS scattering profiles for photon energies where the contrast between polymer and fullerene is enhanced (284.0 eV) and reduced (270.0 eV). (b) Scattering contrast for 2F polymer:PCBM as a function of photon energy near the carbon 1s absorption edge. Contrast of both polymer and fullerene with vacuum are also shown, which quantify mass−thickness variations such as surface roughness. The energy dependence of the total scattering intensity (TSI) matches the energy dependence of the 2F polymer:PCBM contrast function supporting that the measured scatter at 284.0 eV is dominated by contrast between polymer-rich and fullerene-rich domains. For energies where 2F polymer:PCBM contrast is low, scattering is dominated by mass−thickness variations which explains the absence of the broad scattering peak near 0.08 nm^{-1} for 270.0 eV in (a) and the deviation of the TSI from 2F polymer:PCBM contrast near 285 and 289 eV in (b).

tunability of the contrast. For 270.0 eV, the materials contrast between the polymer and PCBM is nearly 1 order of magnitude lower than the pure materials:vacuum contrast (see Figure 9b), meaning that any scattering due to surface roughness/thickness variations will be enhanced. For this energy, only scattering for $q < 0.03$ nm^{-1} is significant, indicative of thickness variations with a spacing greater than 1000 nm. On the other hand, use of an energy near resonance such as 284.0 eV where contrast between the polymer and fullerene is enhanced, scattering peaks are observed near 0.2 nm^{-1} for 0F- and 1F-based blends and around 0.08 nm^{-1} for 2F-based ones. This indicates that the dominant domain spacing for 2F-based blends ($2\pi/q = 85$ nm) is larger than those based on 0F and 1F (35 nm). The increase in domain spacing is representative of an increase in

dx.doi.org/10.1021/ja309289u | J. Am. Chem. Soc. 2013, 135, 1806−1815

domain size, which has also been observed when adding fluorine substituent atoms in other systems.[9,11,17] Atomic force microscopy phase imaging (see SI Figures S17−19) confirms this result where fibrillar structures are noted for the 2F-based blend. Figure 9b also confirms that scattering is dominated by optical contrast between polymer-rich and fullerene-rich domains. By integrating scattering profiles like those in Figure 9a to determine the total scattering intensity (TSI) for multiple energies, it evident that the energy dependence matches that of the contrast between polymer and fullerene. The TSI is also known as Porod's invariant.[53] Importantly, the energy dependence of the TSI does not follow either materials:vacuum contrast functions meaning that surface roughness contributions and thickness variations to the scattering are minimal at 284.0 eV.

Along with ensuring that scattering originates from optical contrast between polymer-rich and fullerene-rich domains, the TSI is related to relative domain purity differences between blends.[54] Since the contrast function for the three blends is nearly equivalent at 284.0 eV (see SI Figure S20), the polymer/fullerene blend ratios are identical, and the scattering has been corrected for differences in active layer thickness, any differences in the TSI are indicative of changes in the relative domain purity over the measured q-range. From Figure 9a, it is evident that the 2F polymer-based blends have the greatest TSI and correspondingly purest domains. Comparing the TSI for this blend to those based on 1F and 0F result in relative purity values of 71% and 66%, respectively. Therefore, not only is the domain spacing similar for the 1F and 0F-based blends, but the domain purity is also comparable. Significantly larger and purer domains are only observed for the 2F-based blends.

The higher purity of the 2F-based blends can be explained in part due to reduced paracrystallinity (Figure 8). However, it is also expected that fundamental interactions between the different polymers and PCBM also drives domain purification during casting and film drying. These differences are quantified by measuring the molecular miscibility of PCBM in each of the three polymers. For this measurement, samples were solvent annealed in a closed container saturated with DCB solvent for three days to reach equilibrium conditions. This leads to PCBM crystals that are tens of microns in size which are reminiscent of thermally annealed blends.[48] Using scanning transmission X-ray microscopy (STXM) at beamline 5.3.2.2 of the Advance Light Source,[55] the remaining PCBM that does not agglomerate into crystals and is molecularly mixed in polymer is quantitatively measured in the polymer matrix. Figure 10 shows X-ray absorption spectra of the depleted polymer matrix along with linear combination fits using the pure polymer and PCBM spectra following previously reported methods.[56] It is found that the miscibility of PCBM in polymer is highest for the 0F polymer at 20.8 ± 0.6% by weight, and reduces to 15.9 ± 0.9% and 11.7 ± 0.5% for 1F and 2F, respectively. In all cases, the initial percentage of PCBM in the blend films is ∼50% as measured during solution preparation and confirmed with STXM measurements of nonannealed films (see SI Figure S21). The trend in miscibility is in agreement with the trend in domain purity where the domain purity increases with fluorine substitution. In other words, the 0F polymer-based blends are the most compatible and have the highest miscibility (i.e., highest molecular mixing), which is consistent with the measurement that they have the lowest domain purity.

The correlations between crystallinity, domain size and purity, and molecular miscibility with the number of fluorine

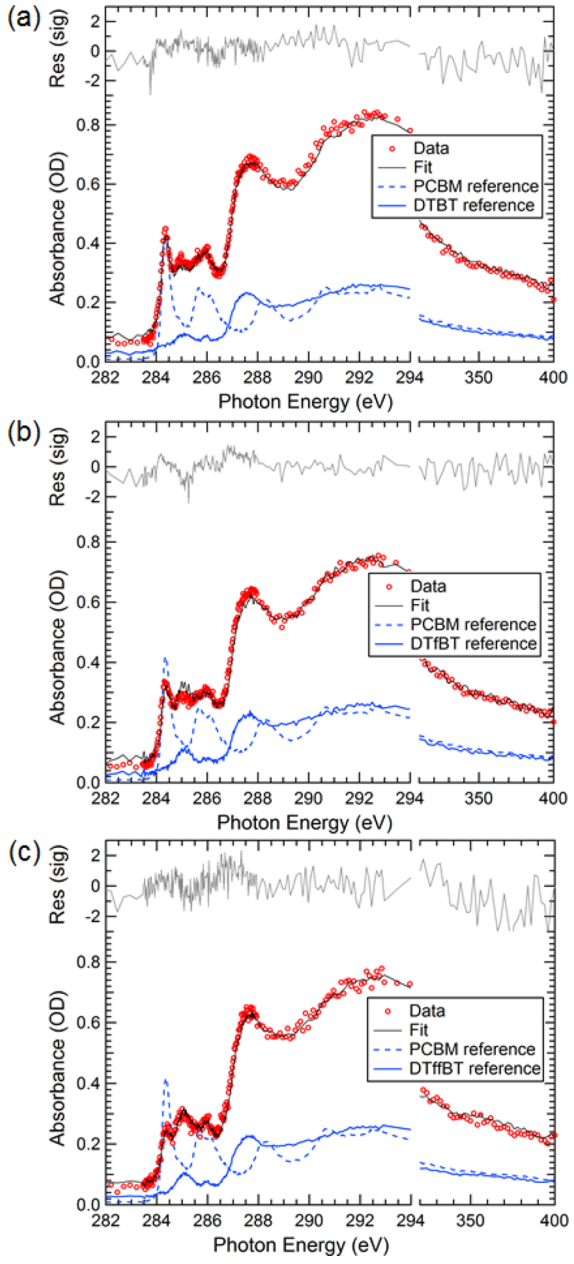

Figure 10. Miscibility of PCBM in (a) 0F, (b) 1F, and (c) 2F thin films that were solvent annealed to equilibrium with corresponding values of 21%, 16%, and 12%. STXM was used to measure the film composition near large PCBM crystals that form after long-term solvent annealing. The initial PCBM percentage by weight prior to annealing was 50% for all blends.

substitutions are quite striking, considering the change in the structure of the repeat unit is very minor (i.e., difference of up to 2 atoms among 150 atoms). Since the polymer crystal orientation and domain size and purity each change with fluorine addition, it is difficult to pinpoint the exact morphological or structural mechanism that dictates performance. Most likely, the performance is a function of each of these traits where molecular interactions play an important role. For example, these morphological and structural features can be linked to a fundamental loss mechanism that reduces the *FF* for 0F- and 1F-based blends: bimolecular recombination. Since both the edge-on polymer crystallite orientation and impure domains in the case of the 0F- and 1F-based devices could

dx.doi.org/10.1021/ja309289u | *J. Am. Chem. Soc.* 2013, 135, 1806−1815

negatively impact charge transport[57] and bimolecular recombination is frequently associated with charge transport, this would explain the higher recombination in both 0F- and 1F-based devices than in the 2F-based ones.

CONCLUSIONS

In summary, we show that adding fluorine substituents to the conjugated backbone can noticeably improve all three key device parameters (V_{oc}, J_{sc}, and *FF*) of polymers-based BHJ solar cells, at least in our studied series ("0F" PBnDT-DTBT, "1F" PBnDT-DTfBT, and "2F" PBnDT-DTffBT). While the increase of V_{oc} can be solely ascribed to the decreased HOMO level by incorporating these fluorine substituents, the improvement on the J_{sc} and *FF* is largely due to suppressed charge recombination by the introduction of these fluorine substituents. The light intensity study discloses a reduced bimolecular recombination by adding fluorine substituents, whereas the hindered geminate recombination is implied by a larger $\Delta\mu_{ge}$ as the number of fluorines increases, with $\Delta\mu_{ge}$ calculated on the basis of the optimized geometry with input of a "true" conformation of alkylated DTBT. Furthermore, adding these fluorine atoms helps improve the morphology and structure in BHJ films. In particular, the doubly fluorinated "2F" polymer shows a greater face-on polymer crystalline orientation and improved $\pi-\pi$ stacking, along with larger polymer/fullerene domains of higher purity. The higher purity, caused by the observed lower miscibility with PCBM as fluorine concentration is increased, likely reduces bimolecular recombination, leading to improved device function. All of these contribute to the overall device efficiency increasing from 4% in the case of the 0F polymer to over 7% for the 2F polymer. Overall, these findings indicate that "fluorine" substitution can have a strong influence on a number of important device parameters and should be considered for use in other photovoltaic polymer systems.

ASSOCIATED CONTENT

Supporting Information

Full experimental section, including detailed synthesis of monomer (DTfBT) and 1F polymer (PBnDT-DTfBT) and their NMR spectra; GPC curve; electrochemical studies of all three polymers; SCLC mobility; additional light intensity study results; complete *I*−*V* curves for all photovoltaic devices; AFM images; pure polymer GIWAXS; soft X-ray polymer/fullerene optical constants; optimized structure coordinates and HOMO/LUMO of the ground state of the monomers; and crystallographic data for three molecules (in CIF format). This material is available free of charge via the Internet at http://pubs.acs.org.

AUTHOR INFORMATION

Corresponding Author

wyou@unc.edu

Notes

The authors declare no competing financial interest.

ACKNOWLEDGMENTS

H.Z. was supported by a NSF CAREER Award (DMR-0954280), and W.L. was supported by Office of Naval Research (N000141110235). A.C.S., S.L., and W.Y. were supported as part of the UNC EFRC: Center for Solar Fuels, an Energy Frontier Research Center funded by the U.S. Department of Energy, Office of Science, Office of Basic Energy Sciences under award number DE-SC0001011. W.Y. is also a Camille Dreyfus Teacher-Scholar. X-ray characterizations and miscibility measurements were supported by DOE, OS, BES, MSE (DE-FG02-98ER45737). R-SoXS data was acquired at beamline 11.0.1.2, GIWAXS data at beamline 7.3.3, and STXM data at 5.3.2.2 of the ALS, a National user facility supported by DOE (DE-AC02-05CH1123). Also acknowledged are David Kilcoyne, Alexander Hexemer, Cheng Wang, and Anthony Young of the ALS (DOE) for assistance with measurements. We also want to acknowledge support for the purchase of instrumentation from UNC EFRC (Center for Solar Fuels, an Energy Frontier Research Center funded by the U.S. Department of Energy, Office of Science, Office of Basic Energy Sciences under Award Number DESC0001011) and UNC SERC ("Solar Energy Research Center Instrumentation Facility" funded by the U.S. Department of Energy Office of Energy Efficiency & Renewable Energy under Award Number DE-EE0003188).

REFERENCES

(1) Liang, Y.; Xu, Z.; Xia, J.; Tsai, S.-T.; Wu, Y.; Li, G.; Ray, C.; Yu, L. *Adv. Mater.* **2010**, *22*, E135.
(2) Zhou, H.; Yang, L.; Stuart, A. C.; Price, S. C.; Liu, S.; You, W. *Angew. Chem., Int. Ed.* **2011**, *50*, 2995.
(3) Price, S. C.; Stuart, A. C.; Yang, L.; Zhou, H.; You, W. *J. Am. Chem. Soc.* **2011**, *133*, 4625.
(4) Li, Z.; Lu, J.; Tse, S.-C.; Zhou, J.; Du, X.; Tao, Y.; Ding, J. *J. Mater. Chem.* **2011**, *21*, 3226.
(5) Chen, H.-Y.; Hou, J.; Zhang, S.; Liang, Y.; Yang, G.; Yang, Y.; Yu, L.; Wu, Y.; Li, G. *Nat. Photonics* **2009**, *3*, 649.
(6) Zhang, Y.; Chien, S.-C.; Chen, K.-S.; Yip, H.-L.; Sun, Y.; Davies, J. A.; Chen, F.-C.; Jen, A. K. Y. *Chem. Commun.* **2011**, *47*, 11026.
(7) Zhang, Y.; Zou, J.; Cheuh, C.-C.; Yip, H.-L.; Jen, A. K. Y. *Macromolecules* **2012**, *45*, 5427.
(8) Peng, Q.; Liu, X.; Su, D.; Fu, G.; Xu, J.; Dai, L. *Adv. Mater.* **2011**, *23*, 4554.
(9) Schroeder, B. C.; Huang, Z.; Ashraf, R. S.; Smith, J.; D'Angelo, P.; Watkins, S. E.; Anthopoulos, T. D.; Durrant, J. R.; McCulloch, I. *Adv. Funct. Mater.* **2012**, *22*, 1663.
(10) Schroeder, B. C.; Ashraf, R. S.; Thomas, S.; White, A. J. P.; Biniek, L.; Nielsen, C. B.; Zhang, W.; Huang, Z.; Tuladhar, P. S.; Watkins, S. E.; Anthopoulos, T. D.; Durrant, J. R.; McCulloch, I. *Chem. Commun.* **2012**, *48*, 7699.
(11) Albrecht, S.; Janietz, S.; Schindler, W.; Frisch, J.; Kurpiers, J.; Kniepert, J.; Inal, S.; Pingel, P.; Fostiropoulos, K.; Koch, N.; Neher, D. *J. Am. Chem. Soc.* **2012**, *134*, 14932.
(12) Zhou, H.; Yang, L.; You, W. *Macromolecules* **2012**, *45*, 607.
(13) Uy, R. L.; Price, S. C.; You, W. *Macromol. Rapid Commun.* **2012**, *33*, 1162.
(14) Son, H. J.; Wang, W.; Xu, T.; Liang, Y.; Wu, Y.; Li, G.; Yu, L. *J. Am. Chem. Soc.* **2011**, *133*, 1885.
(15) Carsten, B.; Szarko, J. M.; Son, H. J.; Wang, W.; Lu, L.; He, F.; Rolczynski, B. S.; Lou, S. J.; Chen, L. X.; Yu, L. *J. Am. Chem. Soc.* **2011**, *133*, 20468.
(16) Rolczynski, B. S.; Szarko, J. M.; Son, H. J.; Liang, Y.; Yu, L.; Chen, L. X. *J. Am. Chem. Soc.* **2012**, *134*, 4142.
(17) Yang, L.; Tumbleston, J. R.; Zhou, H.; Ade, H.; You, W. *Energy Environ. Sci.* **2013**, *6*, 316.
(18) Bijleveld, J. C.; Zoombelt, A. P.; Mathijssen, S. G. J.; Wienk, M. M.; Turbiez, M.; de Leeuw, D. M.; Janssen, R. A. J. *J. Am. Chem. Soc.* **2009**, *131*, 16616.
(19) Müller, C.; Wang, E.; Andersson, L. M.; Tvingstedt, K.; Zhou, Y.; Andersson, M. R.; Inganäs, O. *Adv. Funct. Mater.* **2010**, *20*, 2124.
(20) Tong, M.; Cho, S.; Rogers, J. T.; Schmidt, K.; Hsu, B. B. Y.; Moses, D.; Coffin, R. C.; Kramer, E. J.; Bazan, G. C.; Heeger, A. J. *Adv. Funct. Mater.* **2010**, *20*, 3959.

(21) Osaka, I.; Saito, M.; Mori, H.; Koganezawa, T.; Takimiya, K. *Adv. Mater.* **2012**, *24*, 425.
(22) Chu, T.-Y.; Lu, J.; Beaupré, S.; Zhang, Y.; Pouliot, J.-R.; Zhou, J.; Najari, A.; Leclerc, M.; Tao, Y. *Adv. Funct. Mater.* **2012**, *22*, 2345.
(23) Zhokhavets, U.; Erb, T.; Gobsch, G.; Al-Ibrahim, M.; Ambacher, O. *Chem. Phys. Lett.* **2006**, *418*, 347.
(24) Brabec, C. J.; Cravino, A.; Meissner, D.; Sariciftci, N. S.; Fromherz, T.; Rispens, M. T.; Sanchez, L.; Hummelen, J. C. *Adv. Funct. Mater.* **2001**, *11*, 374.
(25) Gadisa, A.; Svensson, M.; Andersson, M. R.; Inganäs, O. *Appl. Phys. Lett.* **2004**, *84*, 1609.
(26) Mihailetchi, V. D.; Blom, P. W. M.; Hummelen, J. C.; Rispens, M. T. *J. Appl. Phys.* **2003**, *94*, 6849.
(27) Street, R. A. *Appl. Phys. Lett.* **2008**, *93*, 133308.
(28) Mihailetchi, V. D.; Wildeman, J.; Blom, P. W. M. *Phys. Rev. Lett.* **2005**, *94*, 126602.
(29) Shuttle, C. G.; Hamilton, R.; O'Regan, B. C.; Nelson, J.; Durrant, J. R. *Proc. Natl. Acad. Sci. U.S.A.* **2010**, *107*, 16448.
(30) Koster, L. J. A.; Mihailetchi, V. D.; Blom, P. W. M. *Appl. Phys. Lett.* **2006**, *88*, 052104.
(31) Shuttle, C. G.; O'Regan, B.; Ballantyne, A. M.; Nelson, J.; Bradley, D. D. C.; Durrant, J. R. *Phys. Rev. B* **2008**, *78*, 113201.
(32) Carsten, B.; Szarko, J. M.; Lu, L.; Son, H. J.; He, F.; Botros, Y. Y.; Chen, L. X.; Yu, L. *Macromolecules* **2012**, *45*, 6390.
(33) Zhou, H.; Yang, L.; Xiao, S.; Liu, S.; You, W. *Macromolecules* **2010**, *43*, 811.
(34) Barbarella, G.; Zambianchi, M.; Bongini, A.; Antolini, L. *Adv. Mater.* **1992**, *4*, 282.
(35) Fichou, D. *J. Mater. Chem.* **2000**, *10*, 571.
(36) Kono, T.; Kumaki, D.; Nishida, J.-i.; Sakanoue, T.; Kakita, M.; Tada, H.; Tokito, S.; Yamashita, Y. *Chem. Mater.* **2007**, *19*, 1218.
(37) Anant, P.; Mangold, H.; Lucas, N. T.; Laquai, F.; Jacob, J. *Polymer* **2011**, *52*, 4442.
(38) Osaka, I.; Shimawaki, M.; Mori, H.; Doi, I.; Miyazaki, E.; Koganezawa, T.; Takimiya, K. *J. Am. Chem. Soc.* **2012**, *134*, 3498.
(39) Osaka, I.; Abe, T.; Shinamura, S.; Takimiya, K. *J. Am. Chem. Soc.* **2011**, *133*, 6852.
(40) Rieger, R.; Beckmann, D.; Mavrinskiy, A.; Kastler, M.; Müllen, K. *Chem. Mater.* **2010**, *22*, 5314.
(41) Rieger, R.; Beckmann, D.; Pisula, W.; Steffen, W.; Kastler, M.; Müllen, K. *Adv. Mater.* **2010**, *22*, 83.
(42) Becke, A. D. *J. Chem. Phys.* **1993**, *98*, 5648.
(43) Lee, C. T.; Yang, W. T.; Parr, R. G. *Phys. Rev. B* **1988**, *37*, 785.
(44) Credgington, D.; Jamieson, F. C.; Walker, B.; Nguyen, T.-Q.; Durrant, J. R. *Adv. Mater.* **2012**, *24*, 2135.
(45) Hexemer, A.; Bras, W.; Glossinger, J.; Schaible, E.; Gann, E.; Kirian, R.; MacDowell, A.; Church, M.; Rude, B.; Padmore, H. *J. Phys.: Conf. Ser.* **2010**, *247*, 012007.
(46) Cates, N. C.; Gysel, R.; Beiley, Z.; Miller, C. E.; Toney, M. F.; Heeney, M.; McCulloch, I.; McGehee, M. D. *Nano Lett.* **2009**, *9*, 4153.
(47) Rivnay, J.; Mannsfeld, S. C. B.; Miller, C. E.; Salleo, A.; Toney, M. F. *Chem. Rev.* **2012**, *112*, 5488.
(48) Collins, B. A.; Gann, E.; Guignard, L.; He, X.; McNeill, C. R.; Ade, H. *J. Phys. Chem. Lett.* **2010**, *1*, 3160.
(49) He, X.; Collins, B. A.; Watts, B.; Ade, H.; McNeill, C. R. *Small* **2012**, *8*, 1920.
(50) Yan, H.; Collins, B. A.; Gann, E.; Wang, C.; Ade, H.; McNeill, C. R. *ACS Nano* **2012**, *6*, 677.
(51) Swaraj, S.; Wang, C.; Yan, H.; Watts, B.; Lüning, J.; McNeill, C. R.; Ade, H. *Nano Lett.* **2010**, *10*, 2863.
(52) Gann, E.; Young, A. T.; Collins, B. A.; Yan, H.; Nasiatka, J.; Padmore, H. A.; Ade, H.; Hexemer, A.; Wang, C. *Rev. Sci. Instrum.* **2012**, *83*, 045110.
(53) Porod, G. *Colloid Polym. Sci.* **1952**, *125*, 108.
(54) Collins, B. A.; Li, Z.; Tumbleston, J. R.; Gann, E.; McNeill, C. R.; Ade, H. *Adv. Energy Mater.* **2013**, *3*, 65.
(55) Kilcoyne, A. L. D.; Tyliszczak, T.; Steele, W. F.; Fakra, S.; Hitchcock, P.; Franck, K.; Anderson, E.; Harteneck, B.; Rightor, E. G.; Mitchell, G. E.; Hitchcock, A. P.; Yang, L.; Warwick, T.; Ade, H. *J. Synchrotron Radiat.* **2003**, *10*, 125.
(56) Collins, B. A.; Ade, H. *J. Electron Spectrosc. Relat. Phenom.* **2012**, *185*, 119.
(57) Albrecht, S.; Schindler, W.; Kurpiers, J.; Kniepert, J.; Blakesley, J. C.; Dumsch, I.; Allard, S.; Fostiropoulos, K.; Scherf, U.; Neher, D. *J. Phys. Chem. Lett.* **2012**, *3*, 640.